Hindawi Publishing Corporation
International Journal of Photoenergy
Volume 2012, Article ID 365401, 8 pages
doi:10.1155/2012/365401

Research Article

Synthesis of Fe_3O_4/C/TiO_2 Magnetic Photocatalyst via Vapor Phase Hydrolysis

Fuzhi Shi,[1] Yaogang Li,[2] Qinghong Zhang,[2] and Hongzhi Wang[1]

[1] *State Key Laboratory for Modification of Chemical Fibers and Polymer Materials, Donghua University, Shanghai 201620, China*
[2] *Engineering Research Center of Advanced Glasses Manufacturing Technology, MOE, Donghua University, Shanghai 201620, China*

Correspondence should be addressed to Qinghong Zhang, zhangqh@dhu.edu.cn and Hongzhi Wang, wanghz@dhu.edu.cn

Received 14 September 2011; Revised 15 November 2011; Accepted 15 November 2011

Academic Editor: Jiaguo Yu

A core/multi-shell-structured Fe_3O_4/C/TiO_2 magnetic photocatalyst is prepared via vapor phase hydrolysis process. The as-synthesized core/multi-shell-structured composite is characterized by X-ray diffraction (XRD), field emission scanning electron microscopy (FE-SEM), transmission electron microscopy (TEM), high-resolution electron microscopy (HRTEM), N_2 adsorption-desorption isotherm analyses, vibrating sample magnetometer (VSM), and ultraviolet-visible (UV-Vis) absorption spectroscopy. TEM and HRTEM show that well-crystallized anatase TiO_2 nanocrystals are immobilized on the surface of as-prepared Fe_3O_4/C microspheres with dimensions around 200 nm. N_2 adsorption-desorption isotherm analysis shows that the obtained photocatalyst exists disorderedly mesoporous structure. The photocatalytic efficiency of the catalyst in degradation of methylene blue is evaluated, and the Fe_3O_4/C/TiO_2 photocatalyst with low TiO_2 content (37%) has a relatively higher activity than commercial anatase TiO_2. The intermediate carbon layer avoids the photodissolution of Fe_3O_4 effectively, and the recycling property is largely improved due to the existence of magnetic Fe_3O_4 core.

1. Introduction

Titanium dioxide (TiO_2) nanoparticles have inspired scientists for their potential application in treatment of environmental pollutants in wastewater [1–9]. However, there have been two obvious deficiencies in their practical application. One is the wide bandgap of TiO_2 ($\approx$3.2 eV), so only a small ultraviolet fraction of solar light can be used. The other is the separation of nanosized photocatalyst from wastewater, which is too difficult and energy consumptive [10]. Both deficiencies result in the low treatment efficiency and increase the loss of photocatalyst. Doping TiO_2 with foreign element [11, 12] and mixing TiO_2 with sensitizer [13, 14] are two most important ways to enhance the utilizing of sunlight. And the related researches on catalyst immobilization have also attracted wide attention in order to solve the separation and recycle of the suspended TiO_2 nanoparticles [15, 16]. Some researchers have coated TiO_2 over glass, zeolite, and other substrates to avoid the catalyst-recovering step [17–19].

Recently, magnetic photocatalysts have been addressed to resolve the separation of TiO_2 nanoparticles [20–23]. Cheng et al. [22] obtained a core/shell-structured bactericidal photocatalyst with Fe_3O_4 core and TiO_2 shell for bactericidal application. Xuan et al. [23] fabricated Fe_3O_4/TiO_2 hollow spheres through poly(styrene-acrylic acid) (PSA) template method and carried out the photodegradation of RhB as a model reaction to investigate the photocatalytic activity of the hollow photocatalyst. Nevertheless, Beydoun et al. [24] indicated that the photodissolution of Fe_3O_4 would occur during the light irradiation. So the barrier layer between magnetic Fe_3O_4 and TiO_2 was prepared to reduce the negative effects [25–28]. Song and Gao [8] synthesized the bifunctional titania-/silica-coated magnetic spheres and used MB to evaluate their photocatalytic properties. Ye et al. [28] obtained the core/shell-structured Fe_3O_4/SiO_2/TiO_2 magnetic nanocomposites with enhanced photocatalytic activity by combining sol-gel process with calcinations. Presence of silica coating is essential to reduce the negative effect to magnetite during the photocatalytic process [8, 28]. However, Wang et al. [29] indicated that the carbon shell coated on Fe_3O_4 microspheres was more compact than others, so the direct contact can be avoided effectively. Its benefit to protect

the magnetic carriers enhance the photocatalytic activity and extend the lifetime of magnetic photocatalyst.

Herein, we develop a novel and controllable strategy to prepare the unique $Fe_3O_4/C/TiO_2$ core/multi-shell-structured photocatalyst via vapor phase hydrolysis (VPH) process. It is crucial that TiO_2 in the shell is perfectly crystallized without calcination. In VPH method, the water molecules are gently contacting with alkoxide in vapor phase with the advantage of hydrothermal treatment to obtain highly crystallized TiO_2. The size and crystallinity of anatase TiO_2 crystallite in the shell could be tuned by reaction temperature, duration, and the thickness of anatase shell could also be tuned by varying tetrabutyl titanate (TBOT) content. Finally, the photocatalytic degradation of MB was selected as a model reaction to demonstrate the unique advantage in their photocatalytic activity and recycle facet.

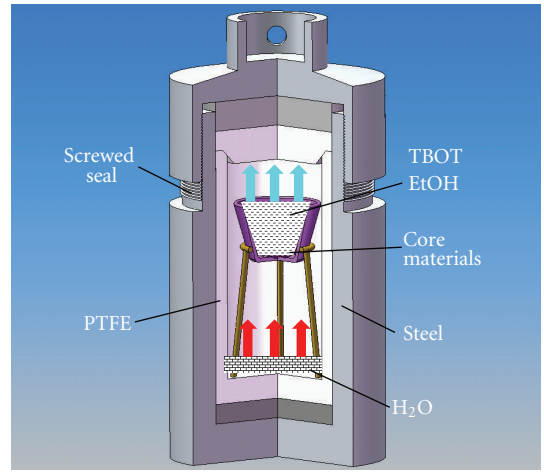

Figure 1: The setup of the vapor phase hydrolysis device.

2. Experimental Procedure

2.1. Materials. Commercial anatase TiO_2, $FeCl_3 \cdot 6H_2O$, ethylene glycol (EG), sodium acetate (NaAc), polyethylene glycol (PEG), oleic acid, cetyltrimethylammonium bromide (CTAB), glucose, TBOT, and absolute ethanol were analytical grade and purchased from Shanghai Chemical Reagent Co., China. All chemicals were used as received without any purification. The distilled water for all processes was purified by ion exchange and then followed by distillation. The specific surface area of commercial anatase TiO_2 is 19 m^2/g and the crystallite size is about 80 nm.

2.2. Synthesis of Fe_3O_4 Microspheres. The ferrite core was first fabricated by solvothermal method, as described by others [30–32]. Typically, 1.35 g $FeCl_3 \cdot 6H_2O$ was dissolved in 50 mL EG to form a clear solution, followed by addition of 3.6 g NaAc and 1.0 g PEG. The mixture was stirred vigorously for 30 min at room temperature and then sealed in a 70 mL Teflon-lined autoclave. The autoclave was heated to 200°C for 12 h. After it was cooled to room temperature, the black products were collected by magnet and rinsed with distilled water and ethanol. The final product was dried under vacuum at 60°C for 8 h.

2.3. Fabrication of Fe_3O_4/C Nanocomposites. The magnetic Fe_3O_4/C nanocomposite was fabricated according to the route of Wang et al. [29]. The reactant mixtures were prepared by dissolving glucose in the aqueous solution containing oleic-acid-stabilized Fe_3O_4 nanoparticles. Typically, 4 g glucose was dissolved in 40 mL oleic-acid-stabilized Fe_3O_4 suspension (2.5 g/L). After that, the mixture was sealed in a 50 mL Teflon-sealed autoclave and heated to 170°C for 3 h. Finally, the product isolated from the mixture by external magnetic field was rinsed with distilled water and ethanol. The final product was dried under vacuum at 60°C for 8 h.

2.4. Preparation of Magnetic $Fe_3O_4/C/TiO_2$ Microspheres. 0.1 g Fe_3O_4/C powders and TBOT were added into 8 mL ethanolic solution and stirred for 2 min to obtain a colloidal solution which was then transferred into the vapor phase hydrolysis device (VPHD, as shown in Figure 1) quickly. 3 mL deionized water was located at the bottom of VPHD as liquid phase to produce vapor at elevated temperature, thus the liquid water did not contact with TBOT directly and the fierce hydrolysis was avoided. The sealed VPHD was heated to different temperature for varying duration. The TBOT content, the reaction temperature, and duration were varied as shown in Table 1. The as-synthesized powder was collected by magnet, rinsed with distilled water and ethanol for several times, and subsequently dried under vacuum at 60°C for 8 h.

2.5. Characterizations. The powder phase composition was identified by X-ray diffraction (XRD) equipment (D/max 2550 PC, Rigaku Co., Japan), using Cu Kα radiation at 40 kV and 200 mA. The crystallite sizes of Fe_3O_4 and anatase are estimated from the corresponding XRD peak at $2\theta = 35.4°$ and $2\theta = 25.3°$ by Scherrer formula ($D = k\lambda/\beta \cos\theta$), where D is the crystallite size, λ is the wavelength of the X-ray radiation (Cu Kα = 0.15406 nm), k is usually taken as 0.89, β is the line width at half-maximum height of the (311) peak of Fe_3O_4 and the (101) peak of anatase after subtracting the instrumental line broadening, and θ is the diffraction angle. The morphology and size of the particles were observed by transmission electron microscope (JEM-2100F, JEOL, Japan) equipped with an energy-dispersive X-ray and field emission scanning electron microscope (S-4800, Hatachi, Japan). The nitrogen adsorption-desorption isotherm was obtained at 77 K using a Autosorb-1 MP (Quantachrome, USA) utilizing Barrett-Emmett-Teller (BET) calculations of specific surface area and Barrett-Joyner-Halenda (BJH) calculations of pore volume and pore size (diameter) distributions from the desorption branch of the isotherm. Magnetic characterization was conducted on vibrating sample magnetometer (6000, PPMS, USA). The carbon content in the Fe_3O_4/C nanocomposites and Sample B is quantitatively measured by Elementar Analyzer (Vario EL III, Elementar, Germany).

Table 1: Summary of the preparative parameters and the specific surface areas.

Sample	Fe_3O_4/C powder (g)	Anatase calculated from TBOT (g)	Temperature (°C)	Time (h)	S_{BET} (m^2/g)
A	0.1	0.125	150	10	57
B	0.1	0.25	150	10	61
C	0.1	0.5	150	10	72
D	0.1	0.25	150	5	58
E	0.1	0.25	150	20	53
F	0.1	0.25	100	10	155
G	0.1	0.25	200	10	39
H	0.1	—	150	10	38

2.6. Photocatalytic Reaction . Ultraviolet (UV) light photocatalytic reactions were carried out to characterize the degradation rate of methylene blue (MB). The suspension was irradiated with a 300 W medium-pressure mercury lamp. First, 0.4 g catalyst (Sample B or commercial anatase TiO_2) was suspended in 500 mL 5.35×10^{-5} M methylene blue (MB) solution. Oxygen was also bubbled into suspension at a flow rate of 100 mL/min during the whole experiment. Prior to photobleaching, the MB-solution-containing catalyst was stirred and stored in dark for 30 min to obtain the saturated absorption of MB. The MB concentration was determined in the sequence of 15, 30, 60, 90, 120, and 180 min using Lambda 35 UV-Vis spectrophotometer (Perkin-Elmer, Waltham, USA) by collecting the absorbance of MB at wavelength of 665 nm.

In order to investigate the recycle property and long-term photocatalytic activity, Sample B was used to degrade MB solutions five times. After ultraviolet light irradiation for 3 h, the magnetic photocatalyst was recycled by external magnetic field, washed three times with deionized water and dried at 105°C for 5 h, the recovered photocatalyst was subsequently used to degrade fresh MB solution under the same irradiation conditions for 3 h. Then 3-cycle, 4-cycle and 5-cycle were also carried out in the same process.

The degradation rate (H) of MB was calculated using $H = C/C_0 \times 100\%$, where C and C_0 are the concentration of remaining MB at different intervals and primal MB solution.

3. Results and Discussion

3.1. X-Ray Diffraction Analysis. The crystallinity and structure of as-prepared Fe_3O_4 particle and Fe_3O_4/C/TiO_2 nanocomposite are confirmed by XRD. As showed in Figure 2, the peak position and relative intensity of Fe_3O_4 (curve a) match well with standard powder diffraction date (JCPDS No. 74-2402), indicating phase purity of Fe_3O_4. Well-resolved diffraction peaks reveal good crystallinity of Fe_3O_4. The average crystallite size of as-prepared ferrite powder estimated by Scherrer formula is around 14 nm, which is in agreement with the result of Zhang et al. [31]. There is no diffraction peaks of carbon appears in curve b due to its amorphous nature and low content compared with Fe_3O_4 and anatase TiO_2. In addition to all diffraction peaks of Fe_3O_4, there are other four diffraction peaks appear at $2\theta = 25.3°$, 37.8°, 48.1°, and 55.1° which correspond to (101), (004), (200), and (211)

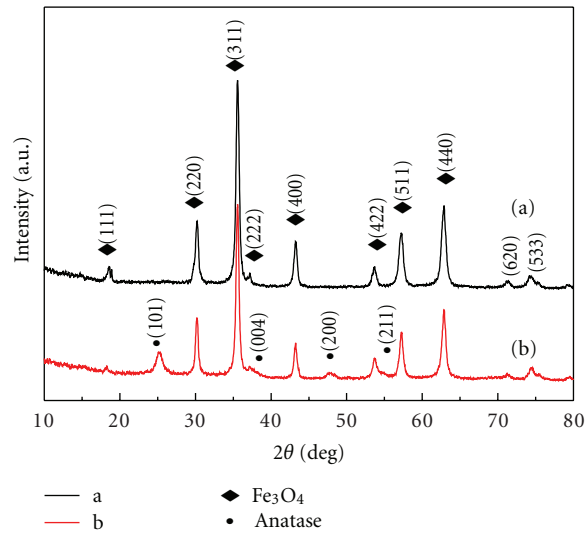

Figure 2: XRD pattern of (a) Fe_3O_4 and (b) Sample B.

planes of anatase TiO_2 (JCPDS No. 21-1272), respectively. The crystallite size of anatase TiO_2 caculated by Scherrer formula is to be ca. 11.2 nm. And the intensity of XRD peaks of Fe_3O_4 has been decreased because there is some carbon and anatase TiO_2 coated on it. XRD results demonstrate that the crystalline anatase TiO_2 and Fe_3O_4 coexist in Sample B.

3.2. Morphology and EDS Analysis. The morphologies of the selected samples are revealed by TEM (Figure 3) and SEM (Figure 4). The Fe_3O_4 crystallites are ultrafine as observed in Figure 3(a) and connect tightly to one another to form spheres. And the diameter of the aggregated particles is around 200 nm (Figure 4(a)). Figure 3(b) shows that amorphous carbon and well-crystallized anatase TiO_2 formed on the surface of Fe_3O_4 microspheres, and the amorphous carbon shell is compact while polycrystalline titania shell is around the carbon shell. The carbon content in the Fe_3O_4/C nanocomposites and Sample B is measured to be 4.4 wt.% and 2.8 wt.%. The crystallite sizes of Fe_3O_4 and anatase TiO_2 are around 15 and 12 nm, which is in agreement with the calculation of XRD. The distances marked in the pattern (Figure 3(c)) between (101) plane of anatase and (311) plane of Fe_3O_4 are 0.35 nm and 0.25 nm, respectively. A well-defined core/multishell structure with Fe_3O_4 as core, carbon

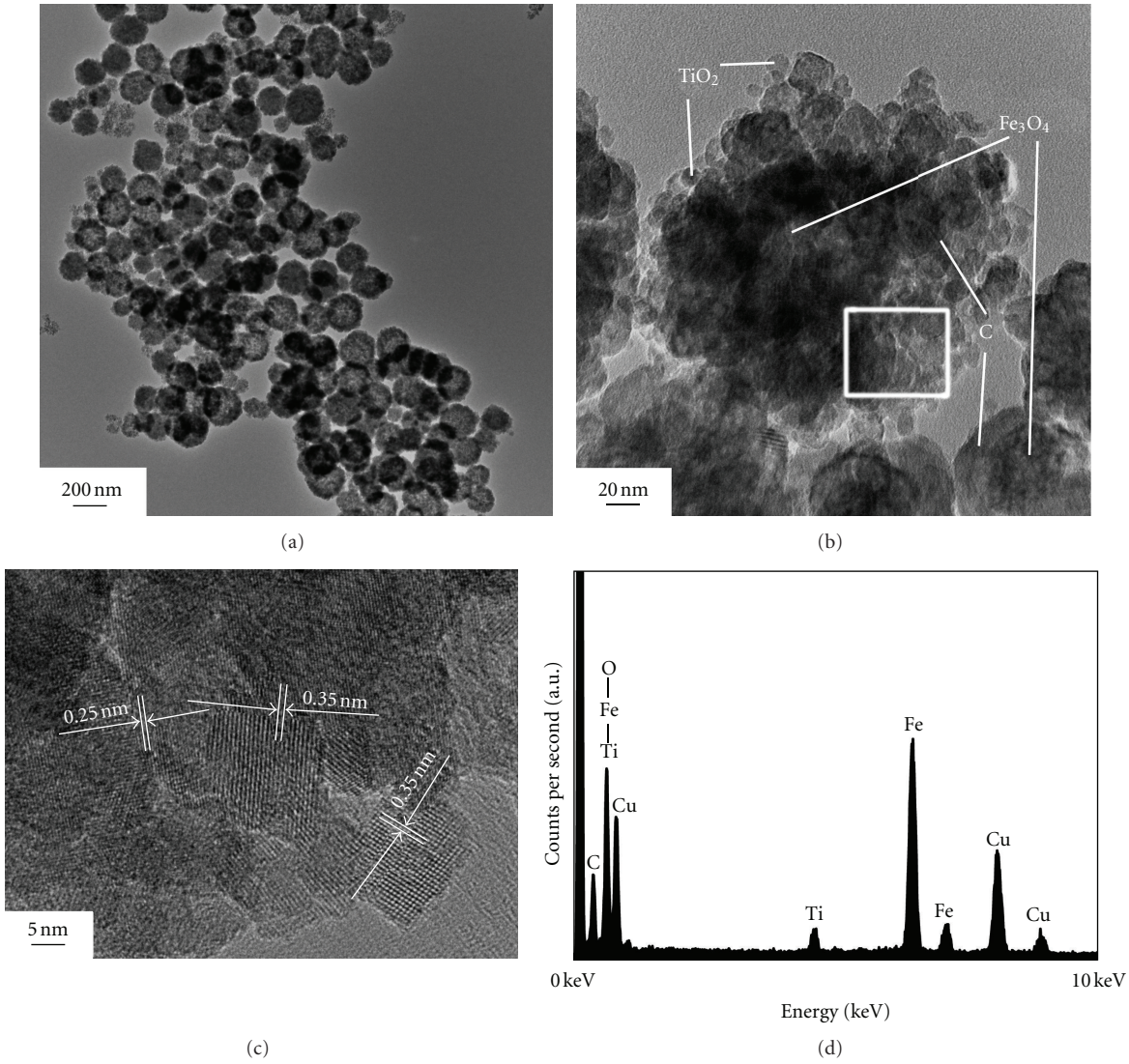

Figure 3: TEM images of (a) Fe_3O_4, (b) Sample B, HRTEM image (c), and EDS result (d) of the selected area in image (b).

as intermediate shell, and anatase as outer shell is indeed formed by the evidence of TEM images (Figures 3(b) and 3(c)). The direct contact between Fe_3O_4 and TiO_2 was inhibited. The EDS results of the selected area in Figure 3(b) are given in Figure 3(d). Ti, Fe, and some C elements come from Sample B; Cu and C come from copper grid and carbon film for TEM analysis. Figure 4 gives the SEM images of the selected samples. It provides more structural information about the three-dimensional morphology of the product. A large quantity of as-prepared Fe_3O_4, carbon-coated Fe_3O_4, and core/multi-shell-structured $Fe_3O_4/C/TiO_2$ with narrow distributions has been synthesized. As shown in Figure 4(b), the greater crosslinking degrees and slickness of the Fe_3O_4/C surface can be seen compared with Figure 4(a) due to the amorphous carbon. Because the small anatase TiO_2 crystallite is coated on the surface of Fe_3O_4/C particles, the result that the surface of Sample B becomes rough can be obtained from Figure 4(c). Up to now, the core/multishell-structured $Fe_3O_4/C/TiO_2$ composite is confirmed by the evidence of SEM and TEM analysis.

3.3. Magnetic Study. The magnetic property of as-prepared Fe_3O_4, Fe_3O_4/C and $Fe_3O_4/C/TiO_2$ is investigated with vibrating sample magnetometer at room temperature. Figure 5 gives the magnetization-hysteresis loops of samples with different composition. It shows that the magnetic saturation value of samples is closely related with the thickness of nonmagnetic shells in given external magnetic field [8]. The magnetic saturation values are 75.1 emu/g for Fe_3O_4 [30], 65.1 emu/g for Fe_3O_4/C, and 56.1 emu/g for $Fe_3O_4/C/TiO_2$ particles. The decrease of saturation magnetization is most likely attributed to the existence of nonmagnetic C and TiO_2 shells on the surface of Fe_3O_4 as shown in curves b and c. Because of the magnetic core, it is notable that these magnetic photocatalysts could be easily recycled from solution

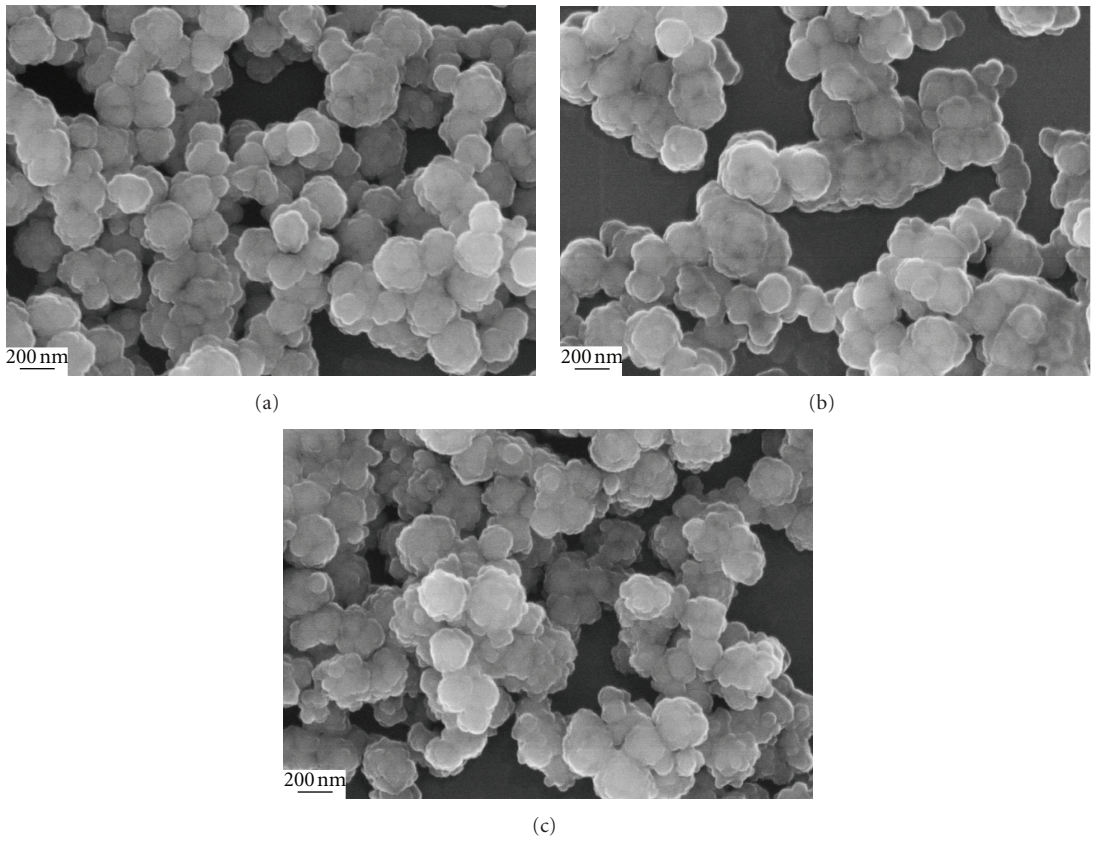

Figure 4: SEM images of (a) Fe_3O_4, (b) carbon-coated Fe_3O_4 microspheres and (c) Sample B.

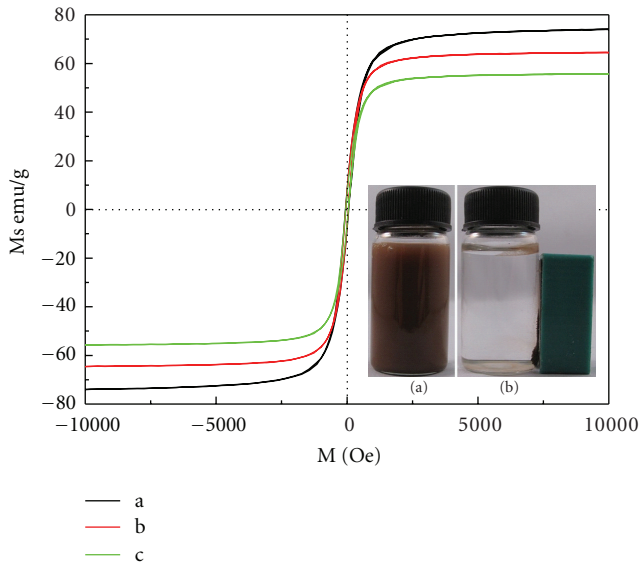

Figure 5: Room-temperature magnetization curves of a: Fe_3O_4; b: Fe_3O_4/C; c: Sample B; Sample B separated from aqueous solution by an external magnetic field (inset).

after treatment by external magnetic field. The inset is the image of Sample B separated from aqueous solution by an external magnetic field (inset). The magnetic photocatalyst (Sample B) is recycled by attracting towards the magnet located in right-hand side of sample vials over a short period, demonstrating the high magnetic sensitivity of as-synthesized magnetic photocatalyst.

3.4. Nitrogen Adsorption-Desorption Analysis. The N_2 adsorption-desorption isotherm (Figure 6(a)) of all four samples presents type-IV-like curve with an H3 hysteresis loop, characteristic of mesopores in the spherical cores and shells. Comparing with Sample H, the hysteresis loop of Sample F is shifted to low P/P_0 direction relatively because small crystallite stacking small intraparticles pores on the surface of Fe_3O_4/C spheres. The hysteresis loops of Sample B, G are also shifted to low P/P_0 direction, but it is not obvious in the Figure 6(a). The hysteresis loop of Samples F, B, and G illustrates the fact that the larger crystallite stacking larger intraparticles pores at elevated temperature. The pore size of Sample F is smaller than that of Sample B. It can be explained that the anatase crystallite prepared under 100°C is ultrafine and cumulates small pores. Figure 6(b) gives the pore-size distribution curves of different samples, confirming a preferred porous structure with pore volumes (V_p) 0.36, 0.32, 0.40, and 0.42 cm^3/g and average pore diameters 68.1, 4.7, 9.5, and 81.5 nm corresponding to Samples H, F, B and G, respectively. The high specific surface area of Sample F (155 m^2/g) is the result of fine anatase crystalline prepared under this temperature. Such a porous structure can promote more adsorption of pollutants.

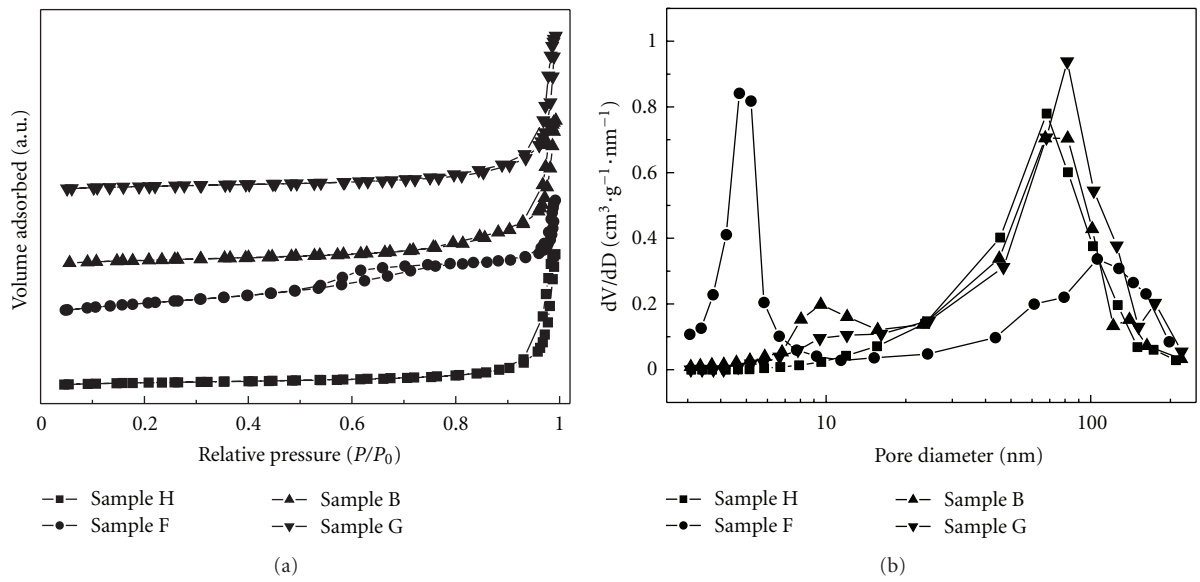

FIGURE 6: N_2 adsorption-desorption isotherm (a) of different samples at 77 K with corresponding pore size distributions (b) calculated by Barrett-Joyner-Halenda (BJH) method from desorption branch. All adsorption-desorption isotherm curves in (a) are added some units along the volume adsorbed axis (Y axis) in order to observe clearly. (■) Sample H, (•) Sample F, (▲) Sample B, and (▼) Sample G.

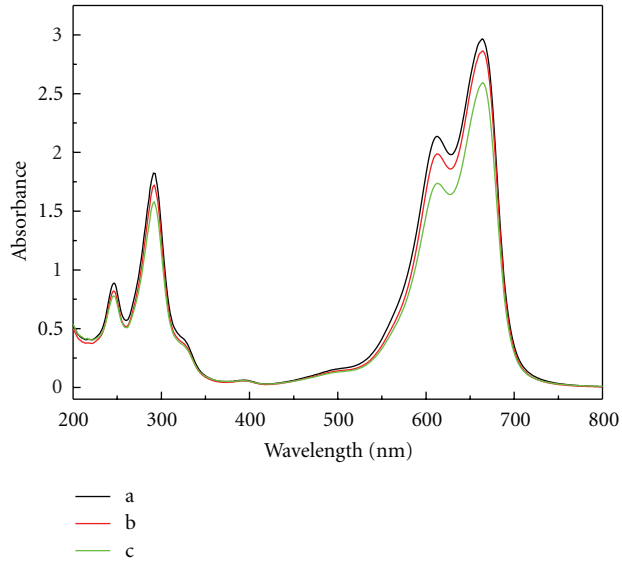

FIGURE 7: The UV-Vis of MB solution after suspending catalysts in dark for 30 min, a: no catalyst; b: commercial TiO_2 and c: Sample B.

3.5. Photocatalytic Activity. Different catalysts are suspended into the MB solution for 30 min in the dark as the adsorption experiment. Figure 7 indicates that the concentration of MB solution is almost no any change (3.33%) in commercial TiO_2 suspension. In contrast, the adsorption of Sample B reaches 12.5%. This adsorption property could increase the local concentration of MB near the titania layer and enhance the photocatalysis efficiency [33]. Figure 8(a) shows the photocatalytic activities of Sample B and commercial anatase TiO_2 in photocatalytic decomposition of MB under ultraviolet light irradiation. As shown in Figure 8(a), the decolorization ratio of MB (control) was less than 20% [34] after 180 min irradiation due to the photodecomposition. Because of the anatase TiO_2 located on the outsurface of $Fe_3O_4/C/TiO_2$ microspheres, it can utilize the light effectively than solid TiO_2 sphere. The TiO_2 content in Sample B is 37%, so the photocatalytic activity of Sample B is relatively higher than that of commercial anatase TiO_2. If the iron oxide directly contacts with a crystalline titanium dioxide phase, electronic interactions between the titanium dioxide coating and the iron oxide core, when the photogenerated electrons in the titanium dioxide phase are transferred into the lower lying conduction band of the iron oxide phase. It is these injected electrons which lead to the reduction of the iron oxide

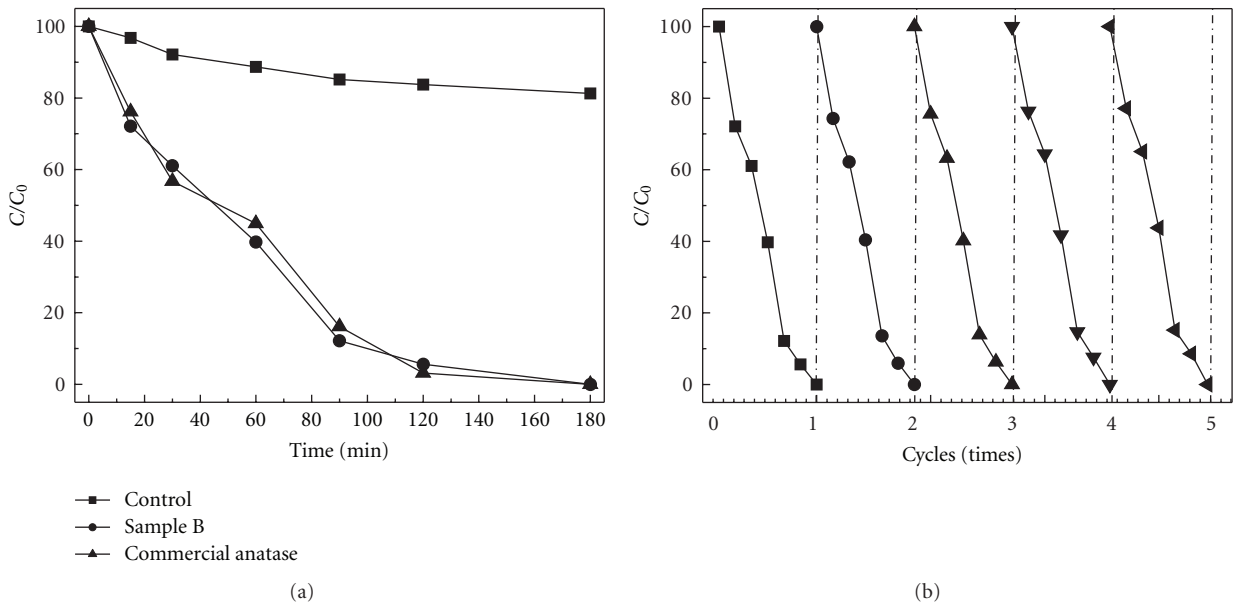

Figure 8: Photocatalytic efficiency of commercial anatase TiO_2 and Sample B to methylene blue (MB); (b) the long-term photocatalytic activity of Sample B.

core, with Fe ions are being formed and migrating to the solution through the porous titanium dioxide coating [24, 33]. So the protection role of intermediate carbon layer is to avoid the direct contact between Fe_3O_4 and titania. Due to the compacted coating with intermediate carbon layer, it can be avoided the electron interaction or photodissolution of Fe_3O_4 probably occurrence of at the point of contact. The long-term photocatalytic activity of Sample B is showed in Figure 8(b). MB is removed completely from the solution in every cycle and photocatalytic degradation efficiency is not varied. Owning to the regenerative property of magnetic photocatalyst and relatively high photocatalytic activity, the $Fe_3O_4/C/TiO_2$ hybrid spheres are well likely to be promising catalyst in the near future.

4. Conclusions

In summary, the core/multi-shell-structured $Fe_3O_4/C/TiO_2$ magnetic photocatalyst has been prepared via a vapor phase hydrolysis process, and the thickness of TiO_2 shell can be tuned from monolayer to several hundred nanometers by varying the TBOT content. The size and crystallinity of anatase TiO_2 crystallite in the shell could be tuned by temperature and duration. The photocatalytic activity of $Fe_3O_4/C/TiO_2$ photocatalyst has relatively higher activity than commercial anatase TiO_2 in photocatalytic degradation of methylene blue (MB) but its recycling property is improved largely. The intermediate carbon layer can avoid the electron interaction or photodissolution of Fe_3O_4 probably occurring at the point of contact effectively.

Acknowledgments

This research was supported by the Opening Project of State Key Laboratory of High Performance Ceramics and Superfine Microstructure (no. SKL201002SIC), the National Natural Science Foundation of China (no. 50772127 and no. 50925312), Shanghai Leading Academic Discipline Project (B603), and the Program of Introducing Talents of Discipline to Universities (no.111-2-04).

References

[1] C. Wang and J. Yao, "Decolorization of methylene blue with TiO_2 sol via UV irradiation photocatalytic degradation," *International Journal of Photoenergy*, vol. 2010, Article ID 643182, 6 pages, 2010.

[2] S.-J. Kim, N.-H. Lee, H.-J. Oh, S.-C. Jung, W.-J. Lee, and D.-H. Kim, "Photocatalytic properties of nanotubular-shaped TiO_2 powders with anatase phase obtained from titanate nanotube powder through various thermal treatments," *International Journal of Photoenergy*, vol. 2011, Article ID 327821, 7 pages, 2011.

[3] G. Dagan and M. Tomkiewicz, "TiO_2 aerogels for photocatalytic decontamination of aquatic environments," *Journal of Physical Chemistry*, vol. 97, no. 49, pp. 12651–12655, 1993.

[4] J. Wang, X. Han, W. Zhang et al., "Controlled growth of monocrystalline rutile nanoshuttles in anatase TiO_2 particles under mild conditions," *CrystEngComm*, vol. 11, no. 4, pp. 564–566, 2009.

[5] J. A. Byrne, P. A. Fernandez-Ibañez, P. S.M. Dunlop, D. M.A. Alrousan, and J. W.J. Hamilton, "Photocatalytic enhancement for solar disinfection of water: a review," *International Journal of Photoenergy*, vol. 2011, Article ID 798051, 12 pages, 2011.

[6] Z. Zhang and J. Gamage, "Applications of photocatalytic disinfection," *International Journal of Photoenergy*, vol. 2010, Article ID 764870, 11 pages, 2010.

[7] X. Song and L. Gao, "Fabrication of hollow hybrid microspheres coated with silica/titania via sol-gel process and enhanced photocatalytic activities," *Journal of Physical Chemistry C*, vol. 111, no. 23, pp. 8180–8187, 2007.

[8] X. Song and L. Gao, "Fabrication of bifunctional titania/silica-coated magnetic spheres and their photocatalytic activities," *Journal of the American Ceramic Society*, vol. 90, no. 12, pp. 4015–4019, 2007.

[9] W.-C. Oh and M.-L. Chen, "The improved photocatalytic properties of methylene blue for V_2O_3/CNT/TiO_2 composite under visible light," *International Journal of Photoenergy*, vol. 2010, Article ID 264831, 5 pages, 2010.

[10] G. Cao, Y. Li, Q. Zhang, and H. Wang, "Hierarchical porous, self-supporting La- and F-codoped TiO_2 with high durability for continuous-flow visible light photocatalysis," *Journal of the American Ceramic Society*, vol. 93, no. 5, pp. 1252–1255, 2010.

[11] Y. Lv, L. Yu, H. Huang, H. Liu, and Y. Feng, "Preparation, characterization of P-doped TiO_2 nanoparticles and their excellent photocatalystic properties under the solar light irradiation," *Journal of Alloys and Compounds*, vol. 488, no. 1, pp. 314–319, 2009.

[12] Y. Lv, Y. Ding, J. Zhou, W. Xiao, and Y. Feng, "Preparation, characterization, and photocatalytic activity of N, S-Codoped TiO_2 nanoparticles," *Journal of the American Ceramic Society*, vol. 92, no. 4, pp. 938–941, 2009.

[13] M. Ruimin, P. Guo, L. Yang et al., "Theoretical screening of -NH_2-, -OH-, -CH_3-, -F- and -SH-Substituted porphyrins as sensitizer candidates for dye-sensitized solar cells," *Journal of Physical Chemistry A*, vol. 114, no. 4, pp. 1973–1979, 2010.

[14] W. J. Youngblood, S. H. Anna Lee, K. Maeda, and T. E. Mallouk, "Visible light water splitting using dye-sensitized oxide semiconductors," *Accounts of Chemical Research*, vol. 42, no. 12, pp. 1966–1973, 2009.

[15] Q. Zhang, W. Fan, and L. Gao, "Anatase TiO_2 nanoparticles immobilized on ZnO tetrapods as a highly efficient and easily recyclable photocatalyst," *Applied Catalysis B: Environmental*, vol. 76, no. 1-2, pp. 168–173, 2007.

[16] Z. Ding, X. Hu, G. Q. Lu, P. L. Yue, and P. F. Greenfield, "Novel silica gel supported TiO_2 photocatalyst synthesized by CVD method," *Langmuir*, vol. 16, no. 15, pp. 6216–6222, 2000.

[17] L. K. Tan, M. K. Kumar, W. W. An, and H. Gao, "Transparent, well-aligned TiO_2 nanotube arrays with controllable dimensions on glass substrates for photocatalytic applications," *ACS applied materials & interfaces*, vol. 2, no. 2, pp. 498–503, 2010.

[18] D. I. Petkowicz, R. Brambilla, C. Radtke et al., "Photodegradation of methylene blue by in situ generated titania supported on a NaA zeolite," *Applied Catalysis A*, vol. 357, no. 2, pp. 125–134, 2009.

[19] T. Kemmitt, N. I. Al-Salim, M. Waterland, V. J. Kennedy, and A. Markwitz, "Photocatalytic titania coatings," *Current Applied Physics*, vol. 4, no. 2–4, pp. 189–192, 2004.

[20] K. F. Ya, Z. Peng, Z. H. Liao, and J. J. Chen, "Preparation and photocatalytic property of TiO_2-Fe_3O_4 core-shell nanoparticles," *Journal of Nanoscience and Nanotechnology*, vol. 9, no. 2, pp. 1458–1461, 2009.

[21] D. G. Shchukin, A. I. Kulak, and D. V. Sviridov, "Magnetic photocatalysts of the core-shell type," *Photochemical and Photobiological Sciences*, vol. 1, no. 10, pp. 742–744, 2002.

[22] T. C. Cheng, K. S. Yao, N. Yeh et al., "Visible light activated bactericidal effect of TiO_2/Fe_3O_4 magnetic particles on fish pathogens," *Surface and Coatings Technology*, vol. 204, no. 6-7, pp. 1141–1144, 2009.

[23] S. Xuan, W. Jiang, X. Gong, Y. Hu, and Z. Chen, "Magnetically separable Fe_3O_4/TiO_2 hollow spheres: fabrication and photocatalytic activity," *Journal of Physical Chemistry C*, vol. 113, no. 2, pp. 553–558, 2009.

[24] D. Beydoun, R. Amal, G. K. C. Low, and S. McEvoy, "Novel photocatalyst: titania-coated magnetite. activity and photodissolution," *Journal of Physical Chemistry B*, vol. 104, no. 18, pp. 4387–4396, 2000.

[25] F. Chen, Y. Xie, J. Zhao, and G. Lu, "Photocatalytic degradation of dyes on a magnetically separated photocatalyst under visible and UV irradiation," *Chemosphere*, vol. 44, no. 5, pp. 1159–1168, 2001.

[26] Z. H. Liao, J. J. Chen, K. F. Yao, F. H. Zhao, and R. X. Li, "Preparation and characterization of nanometer-sized magnetic photocatalyst," *Wuji Cailiao Xuebao/Journal of Inorganic Materials*, vol. 19, no. 4, pp. 749–754, 2004.

[27] T. A. Gad-Allah, S. Kato, S. Satokawa, and T. Kojima, "Role of core diameter and silica content in photocatalytic activity of TiO_2/SiO_2/Fe_3O_4 composite," *Solid State Sciences*, vol. 9, no. 8, pp. 737–743, 2007.

[28] M. M. Ye, Q. A. Zhang, Y. X. Hu et al., "Magnetically recoverable core-shell nanocomposites with enhanced photocatalytic activity," *Chemistry—A European Journal*, vol. 16, no. 21, pp. 6243–6250, 2010.

[29] Z. Wang, H. Guo, Y. Yu, and N. He, "Synthesis and characterization of a novel magnetic carrier with its composition of Fe_3O_4/carbon using hydrothermal reaction," *Journal of Magnetism and Magnetic Materials*, vol. 302, no. 2, pp. 397–404, 2006.

[30] H. Deng, X. Li, Q. Peng, X. Wang, J. Chen, and Y. Li, "Monodisperse magnetic single-crystal ferrite microspheres," *Angewandte Chemie-International Edition*, vol. 44, no. 18, pp. 2782–2785, 2005.

[31] Q. Zhang, M. Zhu, Q. Zhang, Y. Li, and H. Wang, "Fabrication and magnetic property analysis of monodisperse manganese-zinc ferrite nanospheres," *Journal of Magnetism and Magnetic Materials*, vol. 321, no. 19, pp. 3203–3206, 2009.

[32] C. Hou, H. Yu, Q. Zhang, Y. Li, and H. Wang, "Preparation and magnetic property analysis of monodisperse Co-Zn ferrite nanospheres," *Journal of Alloys and Compounds*, vol. 491, no. 1-2, pp. 431–435, 2010.

[33] X. Yu, S. Liu, and J. Yu, "Superparamagnetic γ-Fe_2O_3@SiO_2@TiO_2 composite microspheres with superior photocatalytic properties," *Applied Catalysis B*, vol. 104, no. 1-2, pp. 12–20, 2011.

[34] Z. Wang, L. Mao, and J. Lin, "Preparation of TiO_2 nanocrystallites by hydrolyzing with gaseous water and their photocatalytic activity," *Journal of Photochemistry and Photobiology A*, vol. 177, no. 2-3, pp. 261–268, 2006.